

TI-1916

DO NOT DESTROY
RETURN TO
TECHNICAL DOCUMENT
CONTROL SECTION
WCOSI-3

RECEIVED
SEP 24 1953

PPW

WADC TECHNICAL REPORT 52-226
PART 2

30 16377

5850 CENTRAL FILE

INVESTIGATION OF AXIAL LOADING FATIGUE
PROPERTIES OF HEAT RESISTANT ALLOY N-155

Part 2. An Exploratory Investigation of the Effect of Temperature,
Time, and Stress on Fracture Characteristics
and Metallographic Structure of N-155
and Hardness of N-155 and S-816

Fred W. DeMoney
University of Minnesota

Letter

February 1953

WRIGHT AIR DEVELOPMENT CENTER

20010501002

NOTICES

When Government drawings, specifications, or other data are used for any purpose other than in connection with a definitely related Government procurement operation, the United States Government thereby incurs no responsibility nor any obligation whatsoever; and the fact that the Government may have formulated, furnished, or in any way supplied the said drawings, specifications, or other data, is not to be regarded by implication or otherwise as in any manner licensing the holder or any other person or corporation, or conveying any rights or permission to manufacture, use, or sell any patented invention that may in any way be related thereto.

The information furnished herewith is made available for study upon the understanding that the Government's proprietary interests in and relating thereto shall not be impaired. It is desired that the Judge Advocate (WCJ), Wright Air Development Center, Wright-Patterson Air Force Base, Ohio, be promptly notified of any apparent conflict between the Government's proprietary interests and those of others.

WADC TR 52-226
PART 2

INVESTIGATION OF AXIAL LOADING FATIGUE
PROPERTIES OF HEAT-RESISTANT ALLOY N-155

Part 2. An Exploratory Investigation of the Effect of Temperature,
Time, and Stress on Fracture Characteristics
and Metallographic Structure of N-155
and Hardness of N-155 and S-816

Fred W. DeMoney
University of Minnesota

February 1953

Materials Laboratory
Contract No. AF 33(038)-18903
RDO No. 614-16

Wright Air Development Center
Air Research and Development Command
United States Air Force
Wright-Patterson Air Force Base, Ohio

FOREWORD

This report was prepared by the University of Minnesota under Contract No. AF 33(038)-18903 with the Wright Air Development Center, Wright-Patterson Air Force Base, Ohio, identified by the Research and Development Order No. 614-16, "Fatigue of Aircraft Materials." It was administered under the direction of the Materials Laboratory, Wright Air Development Center, with Captain E. J. Ward acting as project engineer.

The author wishes to extend his gratitude to H. Binder and I. Iwasaki, who did much of the metallographic studies, and to H. Binder and L. C. Lidstrom for carrying out the hardness surveys.

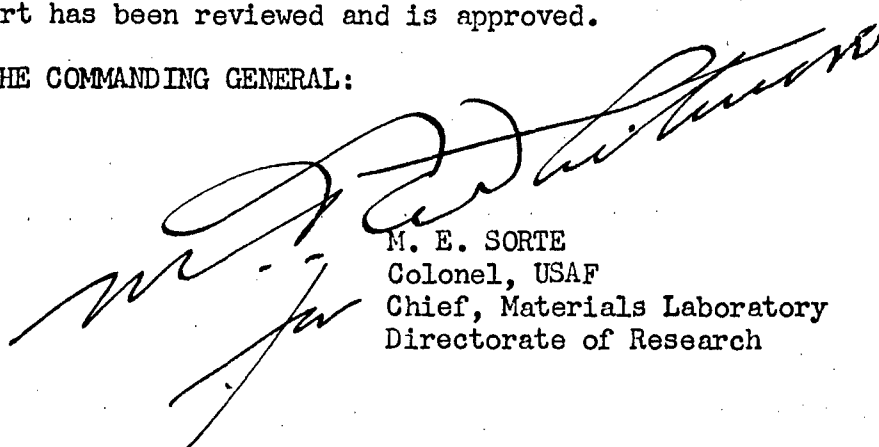
ABSTRACT

An exploratory study of effect of the test variables on the macroscopic appearance of the fracture surface was continued. Fracture profiles were investigated microscopically and an attempt made to quantitatively analyze the nature of the fracture profile. From this analysis is shown that the tendency for an intercrystalline fracture to occur decreases with increasing stress and stress ratio. Investigation of the metallographic structure and hardness of unstressed N-155 verifies prior work concerning the precipitation hardening characteristics of this material. Rockwell "B" hardness tests were conducted on both the surface and longitudinal sections of the stressed specimens in the longitudinal variable stress regions. Tukon Vickers diamond pyramid hardness tests were also conducted on transverse sections of rotating beam fatigue specimens in the transverse variable stress regions. The study of effect of stress variables, while not completely investigated, indicate an acceleration of the precipitation hardening phenomenon as revealed by hardness tests. The acceleration of the precipitation hardening phenomenon is not observed in the metallographic structure of the material.

PUBLICATION REVIEW

This report has been reviewed and is approved.

FOR THE COMMANDING GENERAL:



M. E. SORTE
Colonel, USAF
Chief, Materials Laboratory
Directorate of Research

TABLE OF CONTENTS

Sections	Page
I Introduction and Area of Investigation	1
II Effect of Testing Variables on Macroscopic Appearance of the Fracture	2
III Effect of Testing Variables on the Transcrystalline Versus Intercrystalline Nature of the Fracture Profile	3
3.1 Scope and Testing Procedure	3
3.2 Results and Discussion	5
IV Effect of Testing Variables on Metallographic Structures	7
4.1 Experimental Procedures	7
4.2 Results and Discussion	8
V Effect of Testing Variables on Hardness	12
5.1 Purpose and Scope	12
5.2 Testing Procedure	12
5.3 Results and Discussion	16
VI Summary, Correlation of Data, and Conclusions	20
Bibliography	21
Tables	
I Percent Intercrystalline Fracture	22

LIST OF ILLUSTRATIONS

Figures		Page
1	Macrographs of N-155 Specimens Tested at Room Temperature	23
2	Fracture-Profiles of Specimens Tested at 1500°F	24
3	Fracture-Profiles of Specimens Tested at 1500°F	25
4	Effect of Stress and Stress Ratio on Percent Intercrystalline Fracture of N-155 at 1350° and 1500°F	26
5	Effect of Time and Temperature on Structure and Hardness of N-155	27
6	Effect of Stress and Stress Ratio on Structure and Hardness of N-155	28
7	Effect of Stress and Stress Ratio on Structure of N-155 . . .	29
8	Effect of Time and Temperature on Hardness of N-155 . . .	30
9	Hardness Versus Maximum Stress for Various Times for N-155 at 1350°F Stress Ratio 0.67	31
10	Effect of Combined Mean and Reversed Stress (Stress Ratio 0.67) on Hardness of N-155 Axial Stress Specimens at 1350°F	32
11	Increase in Hardness with Time for Different Levels of Maxi- mum Stress for N-155 at 1350°F and Stress Ratio 0.67. .	33
12	Hardness Versus Stress for N-155 Rotating Beam Specimens at 1350°F	34
13	Hardness Versus Stress for S-816 Rotating Beam Specimens at 900°F	35
14	Effect of Reversed Stress on Hardness of N-155 and S-816 Rotating Beam Specimens at 1350° and 900°F, Respectively	36

AN EXPLORATORY INVESTIGATION OF THE EFFECT OF TEMPERATURE,
TIME AND STRESS ON FRACTURE CHARACTERISTICS
AND METALLOGRAPHIC STRUCTURE OF N-155
AND HARDNESS OF N-155 AND S-816

SECTION I

INTRODUCTION AND AREA OF INVESTIGATION

The purpose of this investigation was to study the effect of the four test variables on the fracture characteristics, metallurgical structure, and hardness of N-155. Also investigated was the effect of these test variables on the hardness of S-816. Three of the variables, temperature, stress magnitude, and stress ratio were independently set at the start of each test whereas the fourth factor, time to failure, was a dependent variable.

The fracture characteristics were studied by: (a) observing the macroscopic appearance of the fracture surface, and (b) critically examining the fracture profile in order to classify the apparent mode of failure with regard to its transcrystalline or intercrystalline nature. The effect of these four test variables on the metallurgical structure was studied by metallographic means. Also, hardness tests were undertaken to provide supplemental information. No attempts were made to identify the microconstituents or to measure the change in certain internal structures.

The N-155 specimens examined in this investigation were those tested previously (1)* at 1350° and 1500°F, and those tested at Minnesota at room temperature. The S-816 specimens were tested in a previous program (1) at 900°F.

*Numbers in parentheses refer to references in the bibliography.

SECTION II

EFFECT OF TESTING VARIABLES ON MACROSCOPIC APPEARANCE OF THE FRACTURE SURFACE OF N-155

An investigation of the macroscopic appearance of the fracture surface of the specimens tested at 1350° and 1500°F was reported previously (1). No additional work of this type was done in this project on specimens tested at these two temperatures.

The specimens which were tested at room temperature were visually examined and representative macrographs were taken for the two stress ratios, $A = 2.0$ and ∞ . These are shown in the upper part of Figure 1 and disclose the presence of fatigue nuclei.

While it would be desirable to correlate size and characteristic appearance of the fatigue nuclei with the test variables, the lack of suitable fracture criteria and standards make such an association extremely difficult at this time. However, it can be observed that at room temperature the fracture surface of specimens subjected to high stress ratios of $A = 2.0$ and ∞ contain fatigue nuclei of varying size and appearance. These results are in agreement with previous works (1) and (2) in which specimens tested above a stress ratio of approximately 0.67 were found to display fatigue nuclei.

Figure 1 shows a macrograph of a tested specimen to indicate an interesting sidelight. This specimen was subjected to 52,900 psi alternating stress and almost immediately after the start of the test was heated by internal damping and, judging from the red color of the test length during the test, attained an estimated temperature of 1500°F. Due to this excessive temperature, the specimen elongated without rupture and stopped the test. A visual examination of the specimen revealed the presence of many surface cracks and a microscopic examination indicated that the surface cracks were intercrystalline but that their growth into the interior of the specimen became transcrystalline a few grains from the outside.

SECTION III

EFFECT OF TESTING VARIABLES ON THE TRANSCRYSTALLINE VERSUS INTERCRYSTALLINE NATURE OF THE FRACTURE PROFILE OF N-155

3.1 Scope and Testing Procedure

In order to determine the nature of the fracture-profile, several specimens were selected to show extremes in transcrystalline and intercrystalline types of fracture. Thus, for each test temperature the specimens selected were, whenever possible, those with the highest and lowest maximum stress at each of the five stress ratios, 18 specimens in all.

The specimens were prepared for examination using the following procedure. In order to preserve the fractured surface of the specimen, a nickel plate was applied by treating the broken halves of the specimen as follows:

- A. The surface was cleaned by pickling for five minutes in cold concentrated hydrogen chloride.
- B. The specimen was plated in a hard nickel solution of the following composition: 180 gm/L nickel sulphate, 25 gm/L ammonium chloride, and 30 gm/L boric acid.

This solution was used at 120°F with a current density of 35 a.s.f. for about four hours. This operation covered the specimen from its fractured end to about the beginning of the threads with a hard plate 0.003 to 0.006 inch thick.

After plating, the specimen was sectioned with a 1/32 inch thick abrasive cut-off wheel parallel to the axis of the specimen and at right angles to the fatigue nuclei. Enough stock was left so that subsequent operations would reveal the surface at the center of the specimen. This section was then mounted in Bakelite and metallographically prepared by rough polishing by hand through a series of emery papers 320 A, 0, 00, and 000 grit. After being washed, the specimen was final polished by hand on a Miracloth covered wheel using 0-2 micron diamond dust as an abrasive and carbon tetrachloride as a coolant lubricant. This procedure produced a flat surface without tearing or pitting and was superior to other mechanical methods tried. Electropolishing as described in previous reports (3) and (4) was tried but abandoned due to unevenness of polishing and pitting. Various etchants as described in the

literature (1), (3), and (5) were tried and several proved successful on some specimens but not on all. Since it was desirable to have a common etchant for all specimens, the one most successful in revealing all the structures was used. The etchant that proved most satisfactory for this work was electrolytic etch of 2 to 10 percent oxalic acid applied for 5 to 10 seconds with 2 1/2 to 4 1/4 volts DC.

Photomicrographs of the complete fracture-profile from edge to edge were then taken at 150X. This required an average of five to ten individual micrographs, which were then mounted together to give a mural of a complete fracture profile.

The object of the fracture profile analysis was to determine the nature of fracture of the specimen and to quantitatively classify this fracture on the basis of a percentage intercrystalline fracture. This analysis was performed by classifying each grain according to its apparent type of fracture. Some help in this classification was obtained by drawing on the mounted micrographs the hypothetical path of intercrystalline fracture along the grain boundaries one grain below the fracture profile. A qualitative comparison between the fractured grains and the hypothetical intercrystalline fracture was then made. However, in order to classify the individual grain according to type of fracture, it was further necessary to define what is meant by "intercrystalline fracture." Ordinarily, intercrystalline means between crystals or along the grain boundaries. Because it is sometimes difficult to identify grain boundaries in the fracture profile because of their indistinctness, the following additional guide was used. If there was an abrupt change in fracture direction at the transverse grain boundaries, then the fracture at that grain is considered intercrystalline.

After this grain-by-grain classification was accomplished, the "percent intercrystalline fracture" was determined. This quantity is defined as the ratio of the length of intercrystalline fracture to the total length of the fracture profile expressed as a percentage. The length of the intercrystalline fracture was determined by measuring the photomicrographs with a map measurer. The total length of the fracture was measured in a similar manner.

This procedure was used in the determination of the percent intercrystalline fracture for the specimens shown in Table I. Although the procedure was generally successful, there were some difficulties, such as determining the nature of fracture of the individual grain. It was extremely

difficult at times to distinguish between a torn grain and an intercrystalline fracture. Other sources of difficulty were: (a) the plastic deformation in the fractures caused by pounding at the fractured ends before the testing machine was stopped (specimen JU-15, for example), and (b) poor definition of grain boundary caused by the etchant (JQ-5).

3.2 Results and Discussion

A representative series of fracture-profiles are shown in Figures 2 and 3. The results obtained from this analysis are shown in Table I and are plotted in Figure 4. Data obtained from a previous investigation (1) are also shown. It is seen that the four test variables--time, temperature, stress, and stress ratio--influence the type of fracture and these effects will be discussed in the following sections.

3.2.1 Effect of Time and Temperature on Fracture-Profile.

In general, the longer the time to fracture, the more likely is the fracture to be intercrystalline in nature. The tendency in short time fractures is towards reduced intercrystalline cracking. With regard to temperature effects, there has been insufficient work to date to be conclusive; but in general, there is a greater tendency towards intercrystalline fracture at the higher temperatures. This finding is in agreement, to a large extent, with that of the previous investigation (1).

3.2.2 Effect of Stress and Stress Ratio on Fracture-Profile.

From Figure 4 it can be seen that at 1500°F the effect of increasing stress for a particular stress ratio is to decrease percentage intercrystalline fracture. This decrease varied with stress ratio but was greatest for a stress ratio of $A = 1.64$ (a specimen exposed to 9000 psi preload stress and $\pm 14,800$ psi alternating stress disclosed a 61 percent intercrystalline fracture and another specimen exposed to $15,000 \pm 24,600$ psi disclosed a 16 percent intercrystalline fracture). Increasing the stress ratio also decreased the intercrystalline nature of the fracture. Considering this relationship on the basis of approximately equal maximum stress, the specimen exposed to a stress ratio of $A = 0$ disclosed a 100 percent intercrystalline fracture, whereas the specimen exposed to a stress ratio of $A = 0.25$ disclosed an 88 percent intercrystalline fracture. Comparing three specimens which had about the same maximum stress of 22,500 psi, but were tested at different stress ratios,

$A = 0$, 1.64, and ∞ , the fracture-profile was 96, 61, and 21 percent intercrystalline, respectively. These findings at 1500°F indicate a difference in results between this investigation and the previous one (1). The essential difference is that transcrystalline fractures were found to occur to a greater extent with greater frequency in the specimens fractured at stress ratios greater than $A = 0$ than was previously reported.

At 1350°F the fracture profile trends were less obvious, but still fairly definite. Considering the effect of stress on the nature of the fracture, it can be seen from Figure 4 and Table I that increasing stress decreases the intercrystalline nature of the fracture. With the limited number of specimens examined, this effect cannot be determined with any degree of certainty in the highest stress ratio. However, the effect of stress ratio on the nature of the fracture can be clearly seen from Figure 4. This shows that increasing the stress ratio decreases the intercrystalline nature of the fracture. This decrease is not quite as great as in the specimens tested at 1500°F, but it is significant. With increasing stress ratio from $A = 0$ to ∞ , the intercrystalline fracture decreased from 100 to 28 percent. The previous investigation (1) shows a similar trend as far as the effect of stress ratio is concerned. A comparison between the two investigations can be made only in the stress ratios of $A = 0$, 0.25, and 0.67, since the higher stress ratios were not investigated in the previous work. This comparison discloses that there is essential agreement in the stress ratio of $A = 0$ and at 0.67, but at $A = 0.25$ the previous report tabulates 100 percent intercrystalline fracture for all specimens, whereas in this report the two specimens are shown to have 77 and 68 percent intercrystalline fracture. This difference may be at best partially associated with how transcrystalline and intercrystalline fractures are defined.

SECTION IV

EFFECT OF TESTING VARIABLES ON METALLOGRAPHIC STRUCTURES OF N-155

4.1 Experimental Procedure

Metallographic studies were made on both the fractured and the threaded end of the specimens tested under various combinations of stress at temperatures of 1350° and 1500°F. The fractured end of the specimen represented the material after exposure to a certain stress magnitude and ratio for a certain time at a certain temperature, whereas the threaded end represented material assumed to be at the same temperature for the same time as the fractured end, but unstressed. The validity of this constant temperature and zero stress assumption is discussed below.

The threaded end selected for metallographic studies lies within 1 inch of the zone in which the furnace was adjusted to maintain a temperature uniform within $\pm 5^\circ\text{F}$ of the test temperature (1). Thus, although the furnace temperature falls off rapidly towards the ends, the reduction in the 1 inch distance cited above is probably not serious.

The assumption of unstressed ends does not, of course, apply to the entire threaded section but only to that material in the ends which is distant from the threads and the test section. This then limits the selection of the area of the threaded ends to a small area near the end of the specimen midway between the roots of the threads and the centerline of the specimen. The stress in this region is considered to be insignificantly small.

The metallographic structure of the fractured end was studied on the same specimens as those used in the fracture-profile investigation and the procedure in their preparation was identical to that described in the preceding section. In addition to these, other specimens representing other stress histories were similarly prepared. The metallographic structure of the unstressed material in the threaded ends of the specimens was also studied and the preparation used was similar to that previously described with the exception that the threaded ends were sectioned without nickel plating.

In the investigation of the effect of the test variables on the precipitation phenomena it is necessary to control the metallographic

preparation closely, particularly the etching conditions. In all cases the etching was carried out with good consistency as follows: 5 percent oxalic acid used electrolytically for 5 seconds at 2 1/2 volts DC.

Structures were studied by a microscopic means using a Bausch and Lomb ILS Metallograph. The fracture structure was observed and representative micrographs taken of an area three to five grains below the surface of the fracture. These micrographs were used to evaluate the effect of stress and stress ratio on the metallographic structure. The threaded ends were similarly examined and micrographs were taken of this representative area. Because these areas were assumed to be at zero stress, these micrographs were used to evaluate the effect of time and temperature on the structure.

4.2 Results and Discussion

The metallographic structure of N-155 in the quenched and aged condition is essentially a two-phase alloy consisting of an austenitic solid solution type matrix and a grain boundary material of the metallic compound type. A third constituent, hereafter termed "Y" which may be a different phase from the two mentioned above, appears as inclusions or stringers throughout the matrix oriented in the direction of rolling of the bar. These compound type constituents have not been identified in this investigation, but other studies, particularly that conducted by Lane and Grant (6), have identified similar constituents as chromium and columbium carbides.

4.2.1 Effect of Time and Temperature on Structure. The effect of two elevated temperatures has been investigated and the results are shown in Figure 5. It can be seen that the grain size is affected very little by temperature or time at temperature. The only change that seems to occur is that the grain size becomes more uniform with increasing time at temperature. There is no evident grain growth or grain coarsening. While the effect of time and temperature on the matrix and grain boundaries is more difficult to ascertain, nevertheless, there are certain changes which can be noted. These changes indicate that the alloy is of the precipitation hardening or age hardening type.

At 1500°F the precipitation begins along the grain boundaries after about 8 hours exposure, as is evident in Figure 5-0, and continues to occur with increasing time. General matrix precipitation occurs after 10 hours.

The size of the precipitate seems to increase with time at temperature, which may indicate continued aging. The grain boundary material appears to decrease in width and lose continuity with increasing time at 1500°F, whereas the constituent "Y" within the matrix appears to remain about the same size and distribution.

At 1350°F precipitation is evident along the grain boundaries in specimens exposed 400 hours. This precipitation continues and tends to agglomerate with increasing time beyond 400 hours. After about 3700 hours the precipitates are structurally resolvable. The grain boundary material appears to remain more or less stable at 1350°F for 3000 hours, but thereafter the constituent may change as shown by Figure 5-E and 5-N. The change is similar to that encountered in the 1500°F exposure and is characterized by a decrease in apparent grain boundary width and a breaking up of the boundary into discontinuous segments. There may be some type of carbide reaction occurring at the grain boundaries as pointed out by Lane and Grant (6). The constituent "Y" within the matrix does not apparently undergo any optically visual change either in size or distribution. Therefore, time and temperature affect the metallographic structure of the unstressed material in a manner which is common to most age or precipitation hardening alloys.

From the observations described above, it may be said that precipitation begins in areas immediately surrounding the grain boundary and then later occurs in the matrix. Grain boundary material apparently reacts with the matrix and after long time exposure may become discontinuous and disappear. The insoluble constituent within the matrix which is recognized by its longitudinal orientation does not appear to change either in size or distribution. These changes are accelerated by an increase in temperature from 1350° to 1500°F.

The interpretation of the structure of precipitation hardening alloys can be influenced by many procedural variables, such as surface polish, etchant techniques, and photographic processes. However, the results of this phase of the investigation as obtained from this interpretation is in agreement with the previous investigation (1) and with Frey et al. (3). The general effect of temperature, that is, 1500°F causes both grain boundary and matrix precipitation in a shorter time than 1350°F, has been realized by all three investigations. Thus, although there is general agreement among investigators, there are some differences found in details. For example,

this study indicates that general matrix precipitation is apparent in specimens exposed 48 hours at 1500°F, whereas the previous investigators found "some" matrix precipitates in specimens exposed 25 hours (1) and others (3) showed this occurred in specimens exposed 100 hours at 1600°F.

4.2.2 Effect of Stress and Stress Ratio on Structure. It has been found that stress, especially cyclic stress, affects precipitation aging in aluminum alloys (7). Thus, it was decided to investigate this effect in temperature resistant alloys. Examinations of several N-155 specimens were undertaken to provide some information on this subject.

The changes that occur in the metallography of this material are shown in Figures 6 and 7. The former illustrates the effect of the highest and the lowest maximum stress for stress ratios of 0, 0.25, and 0.67 on the metallographic structure, whereas the latter shows this effect for stress ratios at 1.67 and ∞ . It is observed in Figure 6 that in the high stress studies at 1350°F, Figure 6 A-D, there is little influence of stress on structures. The precipitation appears in the unstressed material, Figure 6-D, to the same extent that it does in the highest stressed material, Figure 6-C. The low stressed material, Figure 6 E-G, discloses no change in metallography with increasing stress ratio up to 0.67. Evaluating these structures with that of the unstressed material, Figure 6-H, there appears to be no difference between the stressed and unstressed material.

At 1500°F the effect of stress and stress ratio on the structure appears to be in general the same as at 1350°F. Figure 6 I-P shows the change in metallography of specimens exposed to low and high maximum stress at 0, 0.25, and 0.67 stress ratios. The metallographic structure for the high stressed material, Figure 6 I-K, appears to be more or less the same, disclosing medium matrix precipitate and precipitates along the twins. Figure 6-I shows more matrix precipitate than the other three, but this specimen was at temperature about twice as long as the others. The unstressed material, Figure 6-L, reveals a slightly different structure disclosing very slight precipitation in the matrix. The effect of lower stress for the three stress ratios is shown in Figure 6 M-O. These structures have resolvable matrix precipitate and the grain boundaries appear to be broken up into discontinuous network of particles. This grain boundary reaction appears to have been carried out to completion in Figure 6-N, which shows an almost

complete disappearance of the grain boundary phase. An examination of the unstressed material from the same specimen reveals the same grain boundary reaction but to a lesser extent. The unstressed material is shown in Figure 6-P and discloses a resolvable precipitate in the matrix and a slightly discontinuous grain boundary.

When this material is subjected to stress at various stress ratios up to 0.67, the change in the metallographic structure due to stress is very slight, if any. The effect of stress evidently is to produce slip planes and twin bands in the material as a result of plastic strain due to this stress. These planes and bands become preferred regions in which precipitation nuclei can form (8). The resultant structure thus reveals a precipitation along twin bands. However, general matrix precipitation does not appear to be accelerated by stress.

The effect of cyclic stress on precipitation in the higher stress ratios, 1.67 and ∞ , is shown in Figure 7. Again it can be seen that there is little or no difference in the appearance between the stressed and unstressed material. With the exception of the appearance of slip lines and resultant concentration of precipitates along these lines, the structure of the stressed material at $A = 1.67$ appears very similar to the unstressed material. This is true at both 1350° and 1500°F, as can be seen from Figures 7 A-D and I-L. At $A = \infty$ the structures of stressed and unstressed material at 1350°F are almost identical. However, at 1500°F the grain boundary of the stressed material in Figure 7-O appears to be thinner than that in the unstressed material in Figure 7-P. This difference may be attributed to variance in metallographic technique rather than influence of cyclic stress.

The presence of precipitation along slip lines can also be observed in Figures 7-I and 7-M. This indicates that some inelastic deformation occurs even when this material is stressed under high and 100 percent cyclic stress.

SECTION V

EFFECT OF TESTING VARIABLES ON HARDNESS OF N-155 AND S-816

5.1 Purpose and Scope

In order to procure additional evidence regarding the effects of temperature, time, and testing variables on the changes in structure of the material, a series of hardness tests were undertaken on a selection of fractured specimens. It was felt that the relatively rapid and simple hardness test might provide data on trends in structural change which would better guide the metallographic investigation and thus reduce this time-consuming phase of the work. Also, the correlation of structure changes with hardness changes is highly desirable. Furthermore, if some of the structure changes caused by temperature, time, and stress are submicroscopic or otherwise not detectable in the metallographic study, the hardness changes might provide valuable supplemental data.

This study includes: (a) specimens tested under small ratios of alternating direct stress and mean stress since at large stress ratios considerable specimen pounding occurred at fracture which greatly affected specimen hardness, and (b) specimens subjected to reversed bending stress in rotating beam fatigue machines (9). The stress in the test section of the (b) specimens varies from zero at the center to a maximum at the outer fibers. This then provides a means of comparing the quantitative effect of reversed stress only on the hardness (temperature and time variables constant for a given section) by taking hardness readings of the transverse section. Hardness tests on three N-155 (b) specimens tested at 1350°F and two S-816 (b) specimens tested at 900°F were made as discussed below.

5.2 Testing Procedure

5.2.1 Axially Stressed Specimens. Several procedures were tried and are reported below.

5.2.2 Rockwell Tests in Variable Stress Fillet. The Rockwell B hardness was measured at various locations on a fractured specimen. Measurement at the test section, but sufficiently far from the fracture to avoid

localized effects, indicates the hardness of the material after exposure to a specific temperature for a specific time equal to the time to failure under the maximum stress conditions for that specimen. Measurement at various longitudinal locations along the fillet, where the cross-sectional area increases and the stress correspondingly decreases, reveals the hardness of the material exposed to the same temperature and time as above, but at a lower stress. By making measurements at different fillet locations, it was thus possible to procure from one fractured specimen the hardness after a specific time at specific temperature, but at a variety of maximum stresses having the same stress ratio.

Two different approaches, discussed below, were used in measuring the hardness of the test samples.

- (a) Measurements on Original Surface of Fractured Specimen. In this method the oxide film on the surface of the broken specimens was removed by polishing. The specimen was then inserted in a mold which was previously cast using a low melting alloy and the actual test specimen as the pattern. Thus, by rigidly clamping the specimen in the mold, the broken test sample was held securely in place during the hardness measurement. The mold containing the specimen was then inserted in a specially designed and constructed jig which automatically changed the angle of the specimen axis as the specimen was advanced for new hardness tests so that the surface under test was always perpendicular to the hardness penetrator.

The advantage of this method is that no special cutting or other preparation is required for the test specimen prior to hardness measurement. Not only does this provide a rapid method for hardness measurement, but also the fractured surfaces, etc., were retained for future study. However, during use of this method, there was some concern that possible flexibility in the specimen clamping arrangement and jig might be a source of error. Consequently, the hardness measuring method discussed below was also used for checking purposes.

In reporting final data using the above method, the individual hardness readings were corrected for the surface curvature effect according to Lysaght (10).

- (b) Measurement on Sectioned Specimen. In this method the center longitudinal section in the vicinity of the specimen fillet was removed by a thin cut-off wheel under coolant. Hardness was then measured easily at different locations along parallel sides of this section, each location having different stress magnitude. The first section so prepared was also electro-polished to determine whether the cutting-off operation introduced cold work or otherwise affected the hardness. It was found that the hardness before and after removal of approximately 0.004 inch by electro-polishing was not significantly different. Therefore, in subsequent tests the hardness was determined on sections receiving no preparation beyond the cutting-off operation.

5.2.3 Vickers Hardness Measurements on Metallographic Specimens. In an attempt to correlate metallographic structure with hardness, Vickers hardness measurements were made on metallographic specimens of the fractured and threaded ends previously examined in the fracture-profile studies using a Tukon Tester. The fractured ends were measured about 1/16 inch from the fracture and the threaded ends in the area of zero stress as described in a preceding section. A minimum of ten indentations were made for each specimen, the corresponding D. P. H. calculations made and individual readings averaged.

Considerable scatter was found in the individual readings on any one specimen and the calculated sigma variation about the arithmetic mean of these readings varied from 8 to 40. To verify the selection of the 1/16 inch distance from the fractured end as a reliable position, two specimens JN-6 and JX-9 were measured a distance of .250 inch from the fractured end at 0.050 inch intervals. This investigation showed not only considerable scatter in the individual measurements but sigma variation of the mean value from 5 to 15 D. P. H., depending on the distance from the fractured end. While no definite conclusions can be drawn from the results of two specimens, some question as to the reliability of the other hardness data can be raised.

An attempt to correlate these results and others with those of the previous investigations (1) has not proved successful due to insufficient

specimens for direct correlation and also the large variability in hardness of the same specimen.

In view of the scatter and the relatively large variation of the hardness values obtained by this method, the results of this investigation are not presented in this report and this phase of the investigation has been terminated.

5.2.4 Rockwell Superficial 45-T Hardness Tests. These tests were conducted on the threaded ends of all the type "B" specimens tested at 1350° and 1500°F, a total of about 47 specimens. Hardness indentations were made on the ends of the threaded portion on the transverse section after the threaded section had been removed from the specimen by a cut-off wheel. The oxide layer on the end was removed by hand on 30 emery paper and a minimum of three Rockwell Superficial 45-T readings were taken on the ends. These readings were averaged, and this mean averaged with other means of specimens exposed to similar time and temperature conditions. The calculated sigma was 1.0 Rockwell 45-T. From these averages, Figure 8 was constructed which shows the relation of hardness to time for unstressed N-155 at 1350° and 1500°F.

5.2.5 Rotating Beam Specimens. The specimens fractured in the rotating beam fatigue machines were sectioned into transverse discs. Three discs, approximately 0.125 inch thick and 0.205 inch in diameter were cut from one fractured end on a cut-off wheel with coolant. The discs were individually mounted in Bakelite with steel shot to preserve the edges of the specimen.

The mounted discs were first polished by hand on No. 320A, 0, 00, 30, and 40 emery paper then final polished on a Miracloth covered wheel with No. 1 Dymo medium diamond dust as an abrasive and carbon tetrachloride as a coolant. The specimen was electrolytically etched in 10 percent oxalic acid for 5 seconds at 2.5 volts.

Hardness readings were then taken with a Tukon Tester equipped with the Vickers 136° diamond pyramid penetrator and 3000 gram load. The selection of the 3000 gram load was based on a series of experiments designed to determine the load which would show consistent values and would eliminate variations due to the cold worked surface (10). The mounted specimen was placed on the Tukon hardness stage and properly aligned to determine the

center of the disc. The first hardness reading was taken at the center and four readings were made at 0.02 inch increments to the outer surface of the disc. The disc was then rotated at 45° intervals and the centering and hardness reading process repeated so that duplicate readings could be made for averaging purposes. This procedure was repeated for all of the mounted discs. An untested specimen was also sectioned and hardness measurements made in a similar manner for comparison purposes.

Since the stress at any point in the test specimen can be calculated, the hardness versus stress can be plotted.

5.3 Results and Discussion

5.3.1 Rockwell Hardness Tests on Longitudinal Variable Stress Region of Axially Stressed Specimens. The results of these tests, which were performed on nine specimens fractured at a stress ratio A of 0.67 at 1350°F are diagrammed in Figures 9, 10, and 11.

The variation of hardness with maximum stress within each specimen as determined by hardness tests on the sectioned specimen is shown in Figure 9. Each hardness point plotted in Figure 9 is the average of from two to eight individual readings and are reliable to within one R_B hardness number. It should be noted from Figure 9 that in the specimens exposed to temperature for less than about 310 hours, the hardness of each specimen increases with increasing stress magnitude. For specimens exposed about 400 hours there does not appear to be any change in hardness with stress, whereas the specimen exposed about 3350 hours showed a small decrease in hardness with an increase in stress magnitude. Stated differently, the hardness of specimens fractured in less than approximately 310 hours was always a maximum at the minimum area test section and progressively decreased with distance away from the test section along the fillet. This is true of both the measurements made on the original test specimen surface as well as those made on sections cut from the interior of the specimen.

From the original data as plotted in Figure 9, a plot of the iso-stress curves was made as diagrammed in Figure 10. This diagram shows the R_B hardness as a function of number of cycles at stress at 1350°F for each of the three crest stresses* indicated (20,000, 30,000, and 40,000 psi),

*Crest stress refers to the peak or maximum stress which occurs during a stress cycle (1).

the stress ratio being 0.67 in all cases. From the data available it may be assumed that the hardness points plotted in Figure 10 are reliable to within one R_B hardness number.

It should be noted from Figure 10 that the hardness increases with increasing stress at any specific time up to approximately 10×10^7 cycles. Thus, a specimen under a crest stress of 40,000 psi for 2×10^7 cycles has a hardness of 102 R_B , whereas a specimen at 20,000 psi for the same time has a hardness of 99 R_B . After 10×10^7 cycles there is no apparent difference in hardness due to magnitude of stress, and after about 2×10^8 cycles the hardness may decrease. It should also be noted from Figure 9 that there is considerable scatter between hardness points between specimen. Most of this scatter is attributable to the variation between test specimens and is of the same order as the variation in the hardness in the virgin material as indicated in reference 2. Actually, a small correction, based on the hardness variation among bars from which the specimens were cut, was made in the data plotted in Figure 9 to allow for the non-uniformity of the material. In future tests the hardness of each specimen shall be measured prior to test to enable more accurate corrections for non-homogeneity in the virgin material. The hardness difference caused by different stresses within the same specimen is plotted in Figure 11. The hardness increases with increasing stress magnitude are shown as a function of time. Figure 11 reveals the possibility that there may be a maximum hardness produced by a combination of stress and time, and beyond a certain time stress may decrease the hardness.

In spite of the scatter, Figures 10 and 11 show rather well defined trends. In general, the higher the maximum stress (or mean stress) during the stress cycle at fixed stress ratio A and the longer the time at temperature (up to about 500 hours) the harder the material. Of course it is impossible to tell from data at one stress ratio only whether it is the mean stress or alternating stress or some combination of both which causes the spread between the three curves shown in Figure 10.

5.3.2 Tukon Vickers Hardness Tests on Transverse Variable Stress Region of Rotating Beam Specimens. The results of these tests which were performed on three N-155 specimens at 1350°F and two S-816 specimens at 900°F are shown in Figures 12, 13, and 14.

The variation of hardness with maximum stress within each specimen as determined by hardness tests on the sectioned specimen is shown in Figures 12 and 13. Each hardness point plotted is the average of from 8 to 12 hardness readings and although sigma varies from 6.3 to 17.0 D. P. H., a trend can be established. In this respect, the N-155 hardness data disclosed a higher sigma than the S-816 data, thus more confidence can be placed in the S-816 data. The hardness of both unstressed materials not previously exposed to either temperature or stress history does not vary significantly from center to edge (see dashed lines of Figures 11 and 12). The sigma of the hardness readings in the unstressed specimens was about 6.0.

From the original data as plotted in Figures 12 and 13, a plot of the iso-stress curves was made as shown in Figure 14. This shows the effect of reversed stress on the hardness of N-155 and S-816 as a function of the number of cycles at stress. The iso-stress curves for N-155 increases with increasing number of cycles, whereas the high stress iso-stress curves for S-816 apparently attain a maximum. The data for N-155 at 5×10^5 cycles appear to be out of place, but this is due to the choice of "number of cycles" as the abscissa. If the data were plotted on a "time" scale, the points would fall on the curves. (The difference between "time" and "number of cycles" in this case is due to the variable loading frequency common to the rotating beam fatigue test procedure.) This then is an indirect indication of the factor of time at temperature on hardness of N-155. The unstressed curve also demonstrates this factor, for it increases with number of cycles or time.

The "hardening effect" of cyclic stress in N-155 appears to increase with increasing number of cycles, attaining a value of 15 D. P. H. at approximately 9×10^6 cycles. This difference between the hardness of the stressed and unstressed material is statistically significant. It is thought that if the specimens had been stressed at a lower stress and consequently for a higher number of cycles, the hardness curve would show a maximum. This is the case of the specimens tested under axial stress at a stress ratio of 0.67 as discussed in the previous section. Attempts to correlate the results of these two have not been successful because of the lack of reliable hardness conversions between Rockwell "B" and Vickers diamond pyramid for this material. However, it can be seen by inspection that Figures 10 and 14 display the same general curve trends and in both cases hardness increases with stress.

In discussing the results of the investigation of the S-816 material, it must be kept in mind that only two stressed specimens were analyzed and considerable scatter in the observed hardness values occurred although the variance, sigma, was about 6 D. P. H. Consequently, discussions involving specific, finite relationships must be thought of in more general terms.

The damping properties of S-816 at 900°F and N-155 at 1500°F are quite different (11) and therefore one would expect a difference in some other property. This apparently is the case of hardness, for the shape of the S-816 iso-stress curves is different from that of N-155 and contains a maximum which occurs in the higher (50,000 psi and above), but not in the lower stresses. For a stress of 50,000 psi the maximum hardness, 305 V. P. N., occurs at about 10^6 cycles. The "hardening effect" also reaches a maximum which occurs at about 10^6 cycles and amounts to about 20 D. P. H. which is statistically significant. Because of the shape of the unstressed curve, which is almost a straight line and discloses a "negative" hardening effect or softening effect with time, and that of higher stress iso-stress lines, the hardening effect appears to be quite significant. That is, natural aging apparently softens the material, whereas aging under certain cyclic stress conditions increases the hardness to a certain maximum. It is thought that if hardness tests had been made on specimens stressed considerably above the fatigue strength (71,500 psi for 2×10^7 cycles), this effect would have been greater.

SECTION VI

SUMMARY, CORRELATION OF DATA, AND CONCLUSIONS

The nature of the fracture of N-155 tested at 1350° and 1500°F under various combinations of preload and alternating stress has been investigated. It has been observed that the fracture varies from intercrystalline to transcrystalline and this variation is affected by the magnitude of the stress and the stress ratio. Increasing stress and stress ratio apparently decrease the tendency for the fracture to occur intercrystalline. This effect is noticed at both test temperatures.

An investigation of the metallographic structure of the unstressed N-155 material exposed to 1350° and 1500°F for various lengths of time from

4 hours to 4000 hours discloses a precipitation hardening as an important structural transformation. Hardness measurements on this material also indicate this material to be a precipitation hardening alloy. However, hardness measurements indicate that general matrix precipitation may occur before the changes in metallographic structure become microscopically visible.

The effect of stress and stress ratio on the metallographic structure and hardness has been investigated. Stress alone appears to exert a more pronounced effect on hardness than on metallographic structure. In fact, other than the usual deformation markings, such as slip bands, the metallographic structure of N-155 is not affected by stress. From the evidence obtained in this investigation by customary metallographic procedures, it appears that cyclic stress does not accelerate to a significant degree the microscopically visible general matrix precipitation.

Various hardness tests were conducted on longitudinal and transverse sections of axial and rotating bending stressed fatigue specimens of N-155 and S-816. Both materials and both types of fatigue specimens disclose a "hardening effect" which increases with increasing stress and appears to reach a maximum. This "hardening effect" may be due to an accelerating effect of cyclic stress on the precipitation hardening mechanism by the creation of many preferred regions such as slip planes in which the precipitation can occur more readily. Or it may be more simply explained on the basis of the work hardening properties of the austenitic class of alloys, to which N-155 and S-816 belong, since evidence of plastic deformation on both macro and micro scale were observed in these alloys.

BIBLIOGRAPHY

1. F. R. Morral and B. J. Lazan, "Metallographic Studies on N-155 Specimens Exposed to Static and Dynamic Stress at Elevated Temperatures," WADC TR 52-253, December, 1952.

B. J. Lazan and E. Westberg, "Properties of Temperature-Resistant Materials Under Tensile and Compressive Fatigue Stress," WADC TR 52-227, November, 1952.
2. NACA Subcommittee on Heat-Resisting Materials, "Cooperative Investigation of Relationship Between Static and Fatigue Properties of Heat-Resistant Alloys at Elevated Temperatures," NACA No. 51A04, March 7, 1951.
3. D. N. Frey, J. W. Freeman and A. E. White, "Fundamental Effects of Aging on Creep Properties of Solution-Treated Low Carbon N-155 Alloy," NACA Technical Note 1940, August, 1949.
4. University of Minnesota, "Dynamic Creep, Rupture, Elasticity and Damping Properties of Materials and Structures," A. F. Contract No. 33(038)-18903 Progress Report 51-1, September 15, 1951.
5. F. S. Badger, Jr. and F. C. Kroft, Jr., "Cobalt-Base and Nickel-Base Alloys for Ultra-High Temperature," Metals Progress, September, 1947, pages 394-402.
6. J. R. Lane and N. J. Grant, "Carbide Reactions in High Temperature Alloys," ASM Preprint No. 10, 1951.
7. R. F. Hanstock, "The Effect of Vibration on a Precipitation-Hardening Aluminum Alloy," Journal of the Institute of Metals, Vol. 74, Part 9, 1948.
8. R. F. Mehl and L. K. Jetter, "The Mechanism of Precipitation from Solid Solution. The Theory of Age Hardening." Age Hardening of Metals, American Society of Metals, 1940.
9. B. J. Lazan, "A Study with New Equipment of the Effects of Fatigue Stress on the Damping Capacity and Elasticity of Mild Steel," Transactions, ASM Vol. XLII, 1950, pages 499-549.
10. V. E. Lysaght, "Indentation Hardness," Reinhold Publishing Corp., 1949.
11. B. J. Lazan and L. J. Demer, "Damping, Elasticity, and Fatigue Properties of Temperature-Resistant Materials," Proceedings of the ASTM, Vol. 51, 1951.

TABLE I. PERCENT INTERCRYSTALLINE FRACTURE

Specimen Number	Stress Ratio A	Maximum Stress S_c in KSI	Test Temp. °F	Hours to Rupture	Percent Intercrystalline Fracture	
					Minnesota	Syracuse (1)
JZ-16	0	17.5	1350	3185.	100	100
JJ-6	0	40.0	1350	4.	91	100
JI -5	0	11.0	1500	1004.	100	100
JB-5	0	22.5	1500	20.7	96	100
JQ-5	0.25	21.9	1350	3789.	77	100
JN-6	0.25	46.2	1350	7.6	68	100
JR-10	0.25	11.0	1500	4117.	88	100
JW-4	0.25	30.0	1500	8.	54	100
JQ-14	0.67	29.2	1350	3349.	77	?
JK-5	0.67	48.3	1350	11.3	60	82
JS-5	0.67	13.3	1500	4066.	86	100
JV-13	0.67	37.0	1500	10.9	41	59
JV-15	1.64	40.9	1350	23.5	60	?
JY-9	1.64	23.8	1500	1273.	61	Little
JR-14	1.64	39.6	1500	0.4	16	47
JO-5	∞	37.9	1350	0.067	28	?
JX-9	∞	21.8	1500	1048.	21	30
JS-14	∞	25.4	1500	8.3	11	40



JT-22

52.9
0.35

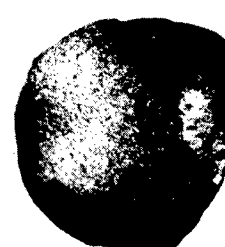
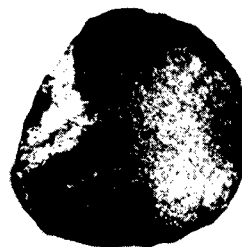
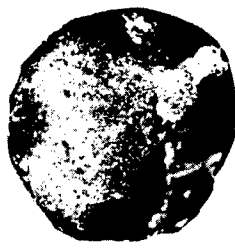
$A = \infty$

MAX STRESS S_c IN KSI
TIME TO FRACTURE, Hrs
5X MAG

JW-21

47.0
32.5

AFTER PREVIOUS STRESS
HISTORY OF 502 HOURS
AT $\pm 44,200$ PSI



JF-20

65.4
18.2

$A = 2.0$

MAX STRESS S_c IN KSI
TIME TO FRACTURE, Hrs
5X MAG

JB-23

63.7
152.7



JP-19

$A = \infty$

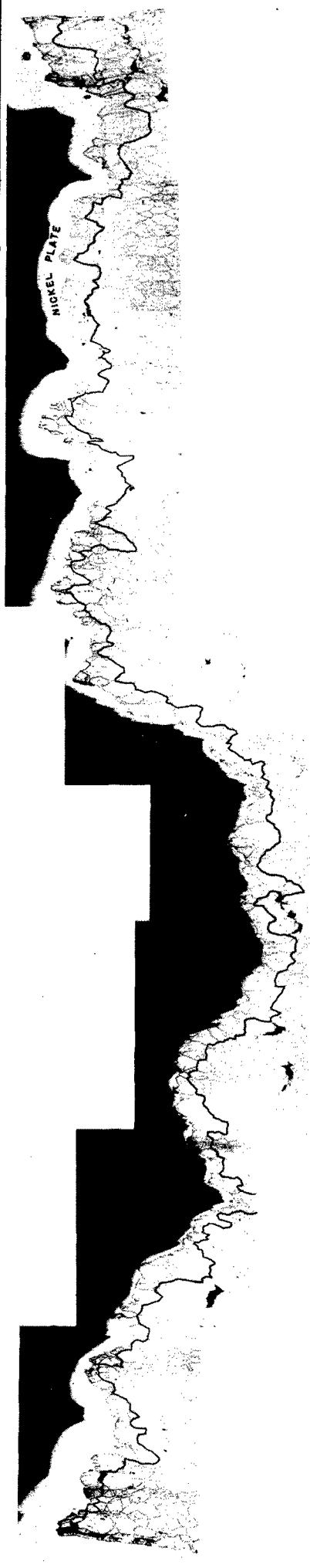
MAX STRESS S_c IN KSI 52.9
3X MAG

SPECIMEN RAPIDLY HEATED BY DAMPING TO APPROX 1500°F. TEST
STOPPED AFTER .08 HOUR DUE TO EXCESSIVE ELONGATION.

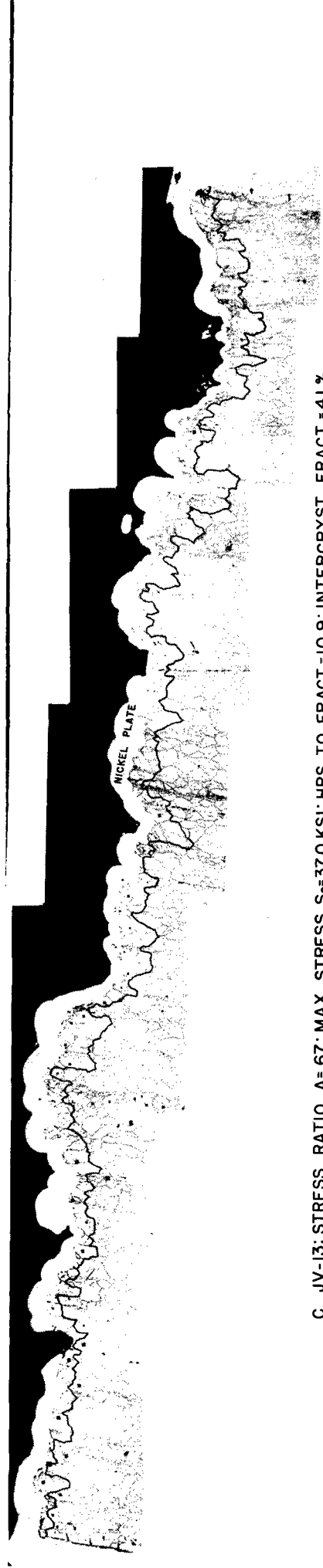
FIG. I. MACROGRAPHS OF N-155 SPECIMENS
TESTED AT ROOM TEMPERATURE



A. JB-5: STRESS RATIO A=0: MAX. STRESS $S_c=22.5$ KSI: HRS. TO FRACT.=20.7: INTERCRYST. FRACT.=96 %



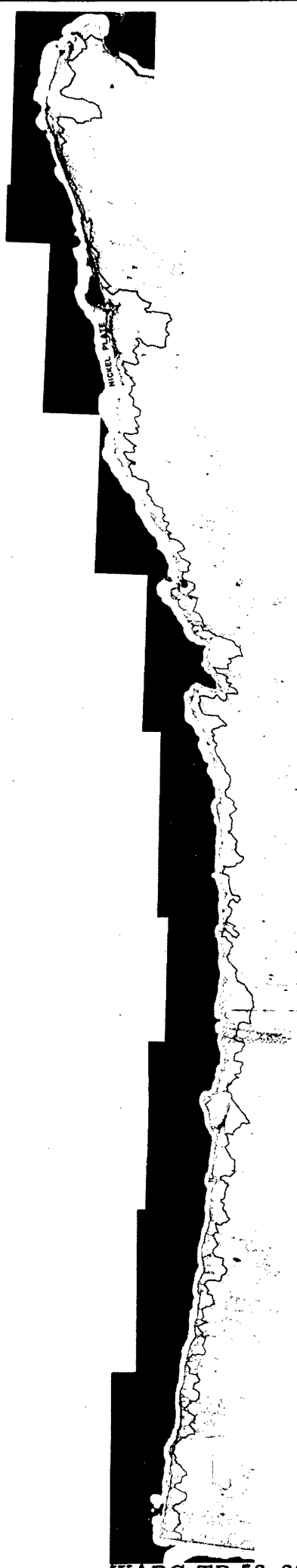
B. JW-4: STRESS RATIO A=25: MAX. STRESS $S_c=30.0$ KSI: HRS. TO FRACT.=8.0: INTERCRYST. FRACT.=54 %



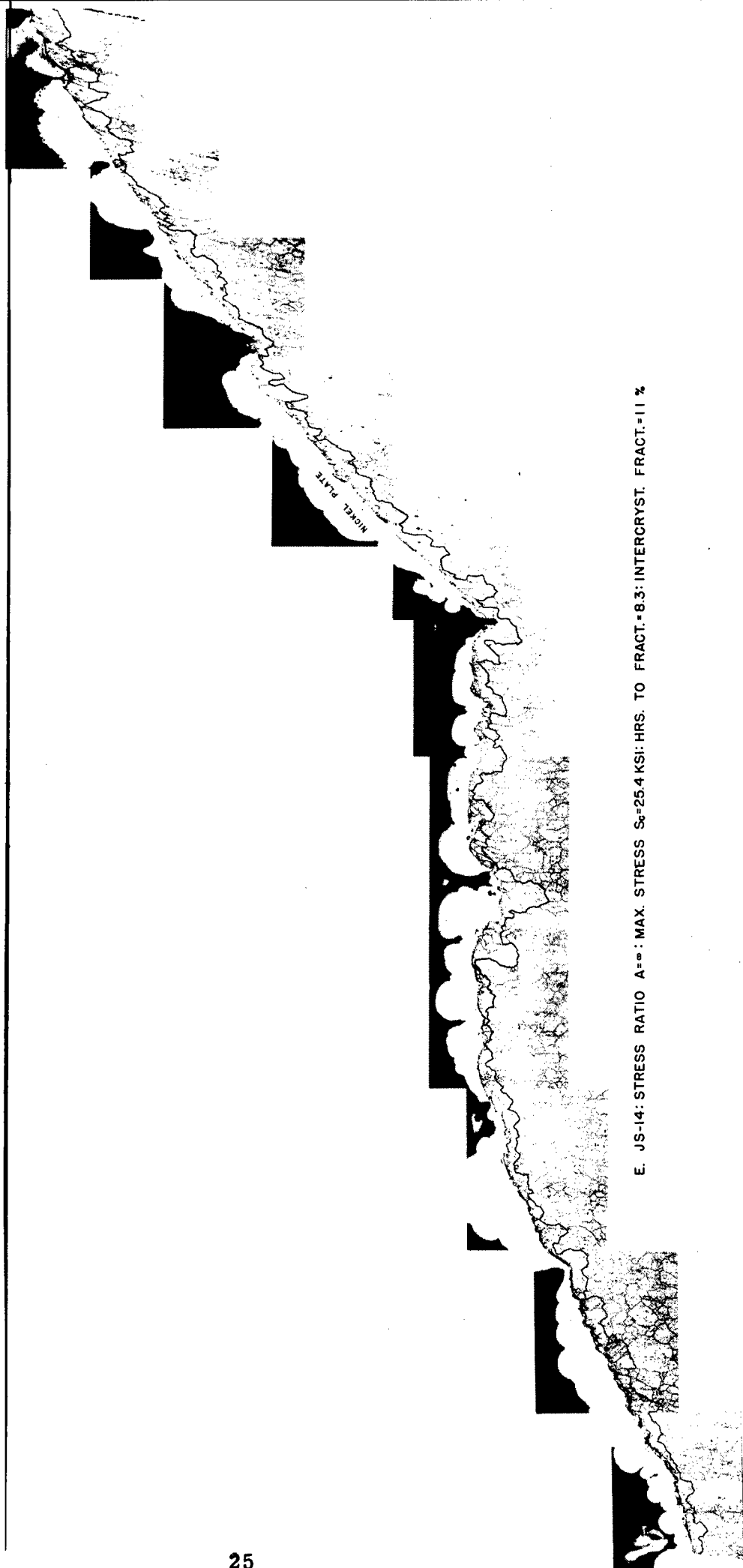
C. JV-13: STRESS RATIO A=67: MAX. STRESS $S_c=37.0$ KSI: HRS. TO FRACT.=10.9: INTERCRYST. FRACT.=41 %

FIG.2 FRACTURE-PROFILES OF SPECIMENS TESTED AT 1500°F. ORIGINAL MAG. 150 X

01"



D. JR-14: STRESS RATIO $A=1.64$: MAX. STRESS $S_c=39.6$ HRS. TO FRACT.-0.4: INTERCRYST. FRACT.-16 %



E. JS-14: STRESS RATIO $A=1.64$: MAX. STRESS $S_c=25.4$ KSI: HRS. TO FRACT.-8.3: INTERCRYST. FRACT.-11 %

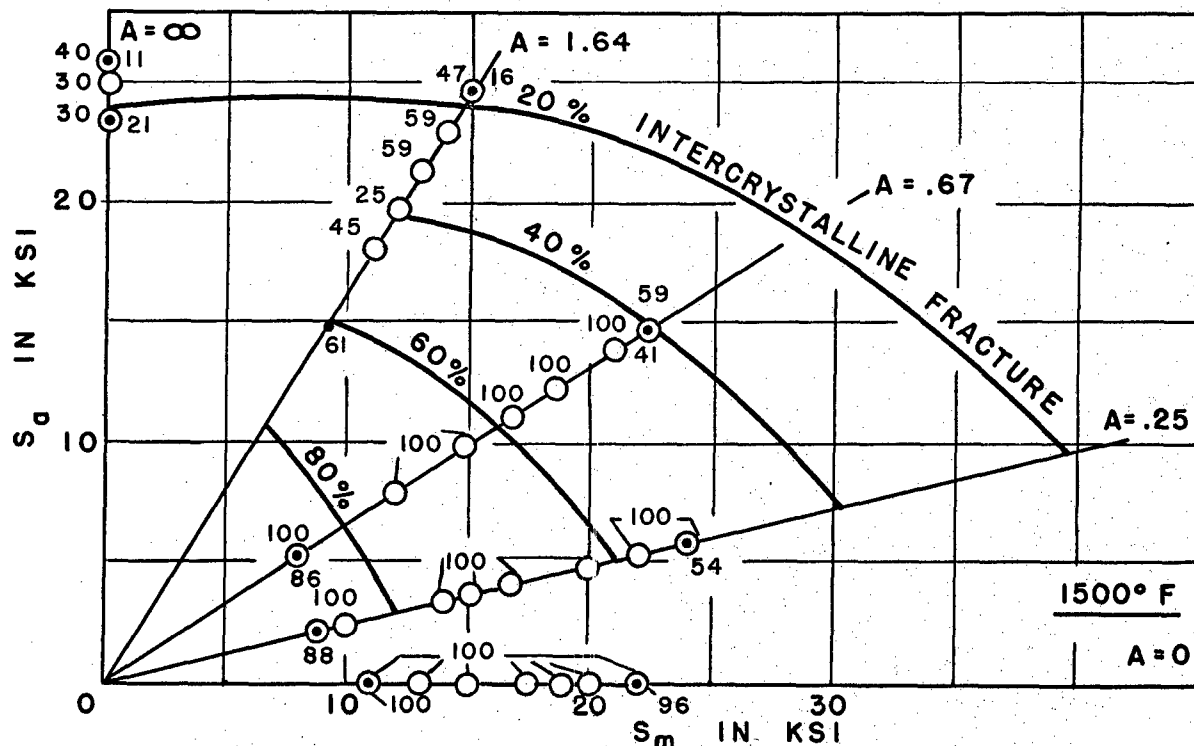
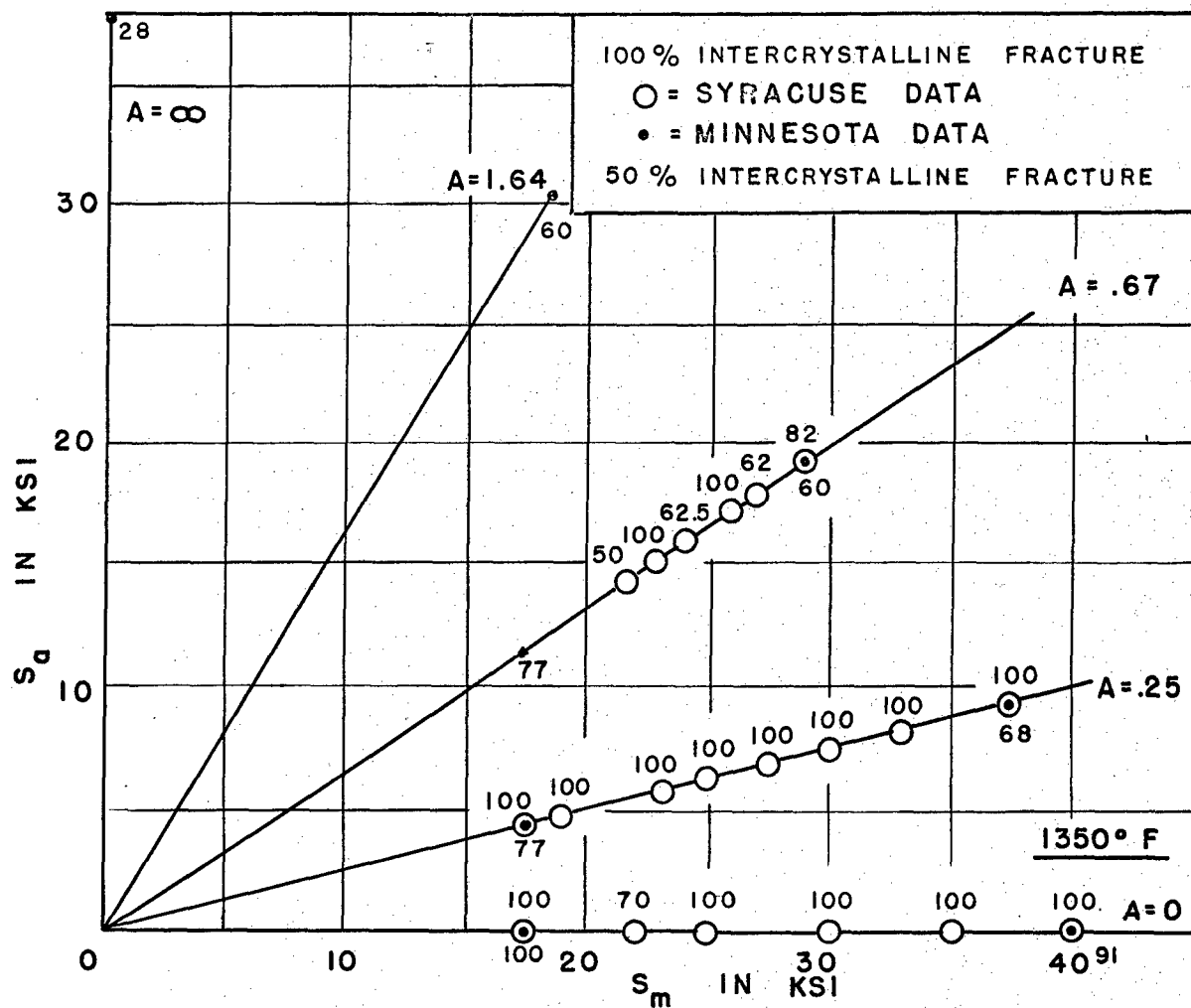


FIG. 4. — EFFECT OF STRESS AND STRESS RATIO ON PERCENT INTERCRYSTALLINE FRACTURE OF N-155 AT 1350° AND 1500° F.

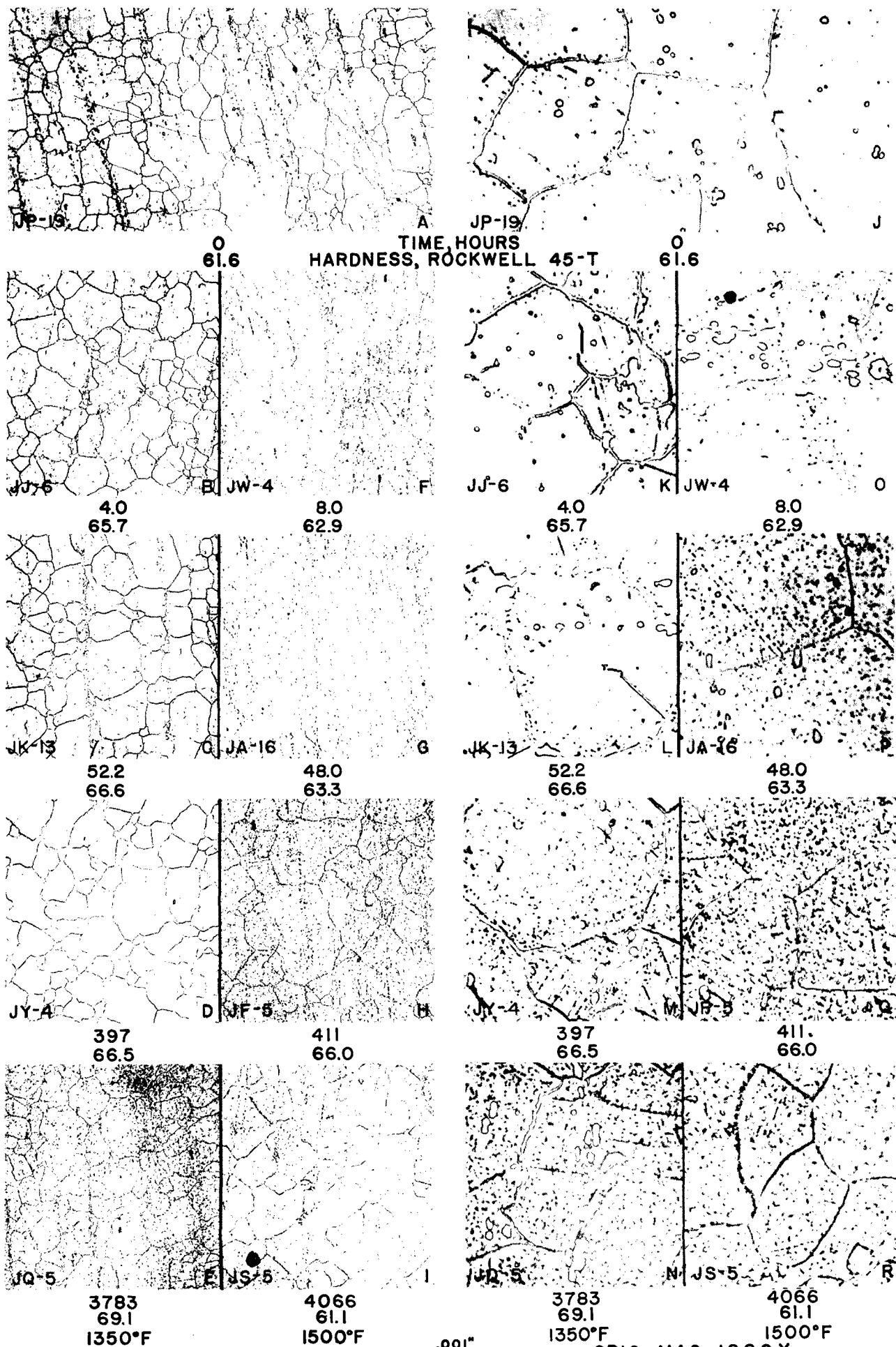


FIG. 5 EFFECT OF TIME AND TEMPERATURE ON
STRUCTURE AND HARDNESS OF N155

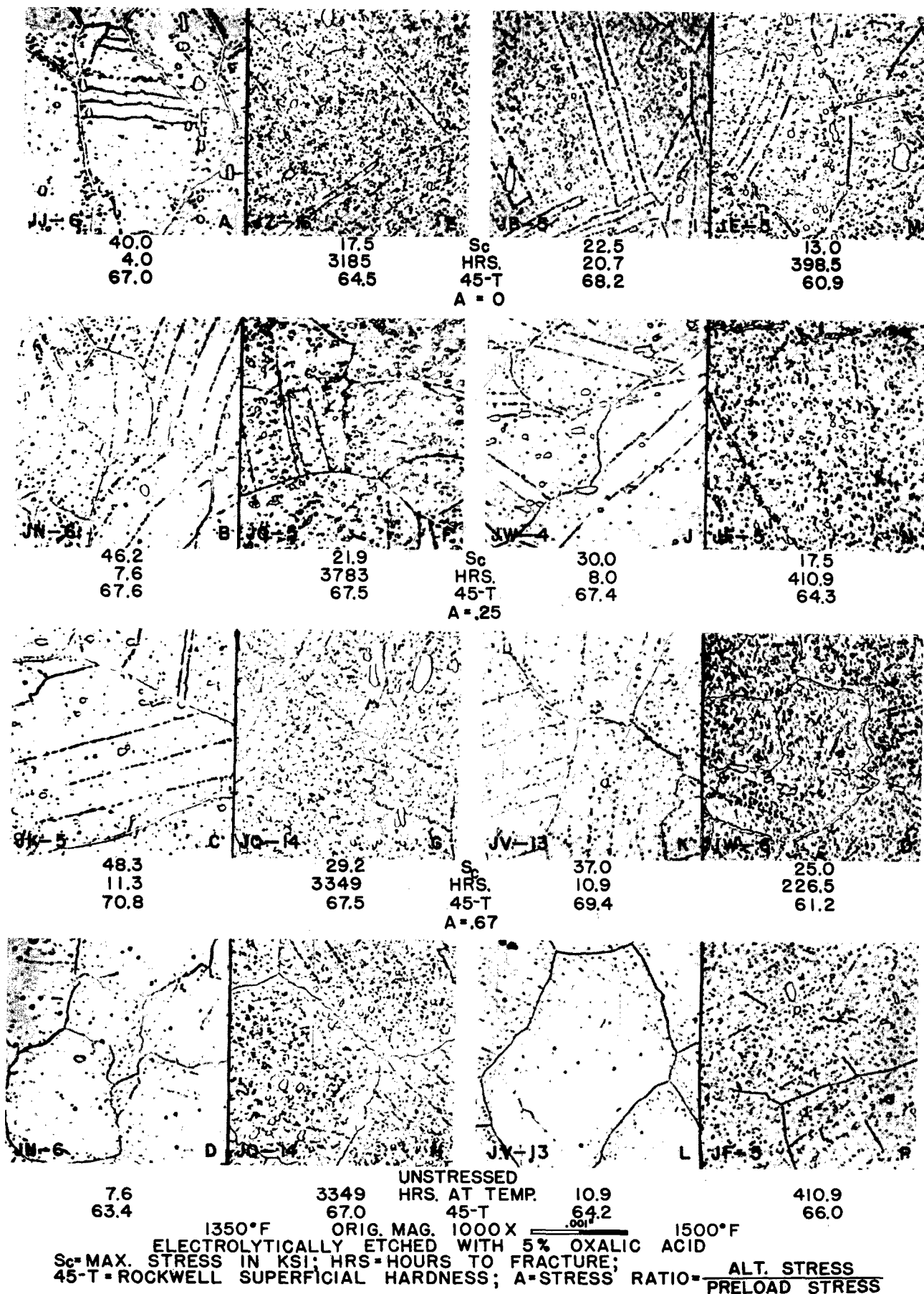
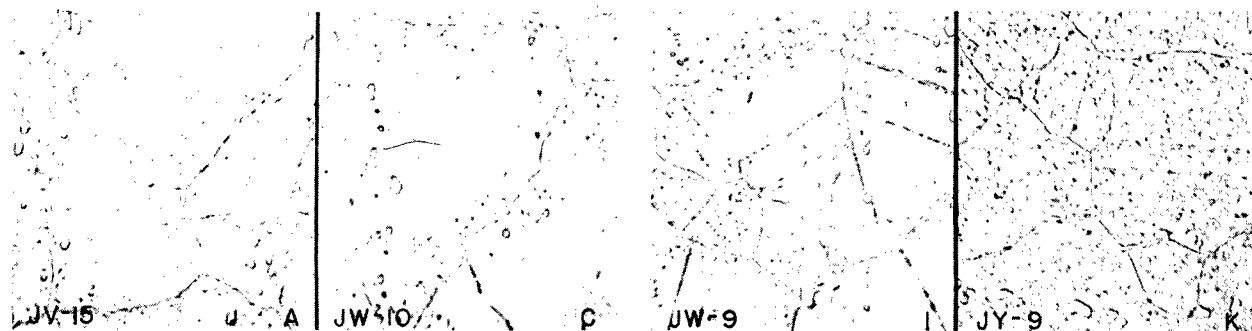


FIG.6. EFFECT OF STRESS AND STRESS RATIO ON STRUCTURE AND HARDNESS OF N-155



47.5
23.5

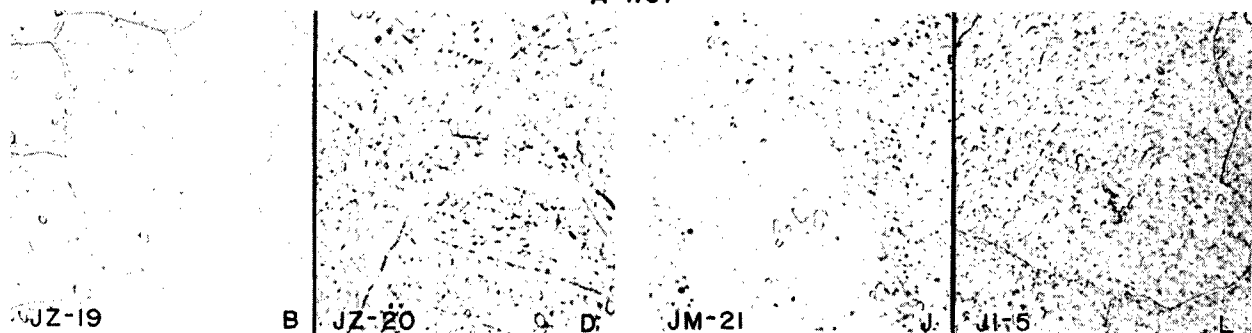
42.2
308.0

Sc
HRS

37.0
14.7

23.8
1273.0

A=1.67



23.0

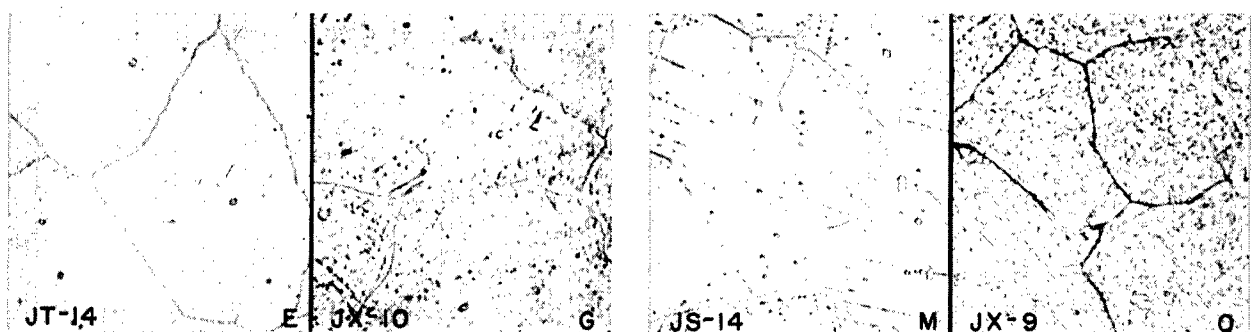
303.0

UNSTRESSED

HRS AT TEMP

14.9

1004.0



38.8
.03

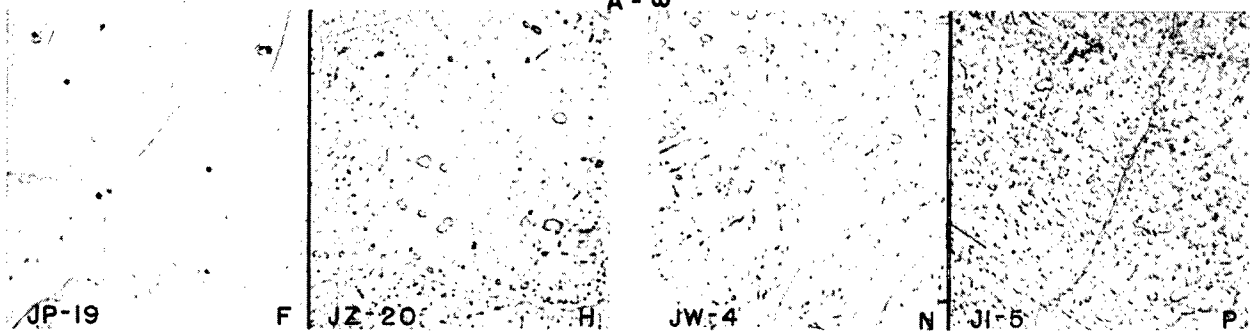
33.6
315.0

Sc
HRS

25.4
8.3

21.8
1048.0

A = ∞



.03

303.0

UNSTRESSED

HRS AT TEMP

8.0

1004.0

1350°F ORIG. MAG. 1000 X .001" 1500°F
ELECTROLYTICALLY ETCHED WITH 5% OXALIC ACID
Sc=MAX. STRESS IN KSI; HRS=HOURS TO FRACTURE
ALT. STRESS
A=STRESS RATIO=PRELOAD STRESS

FIG. 7. EFFECT OF STRESS AND STRESS RATIO ON STRUCTURE OF N-155

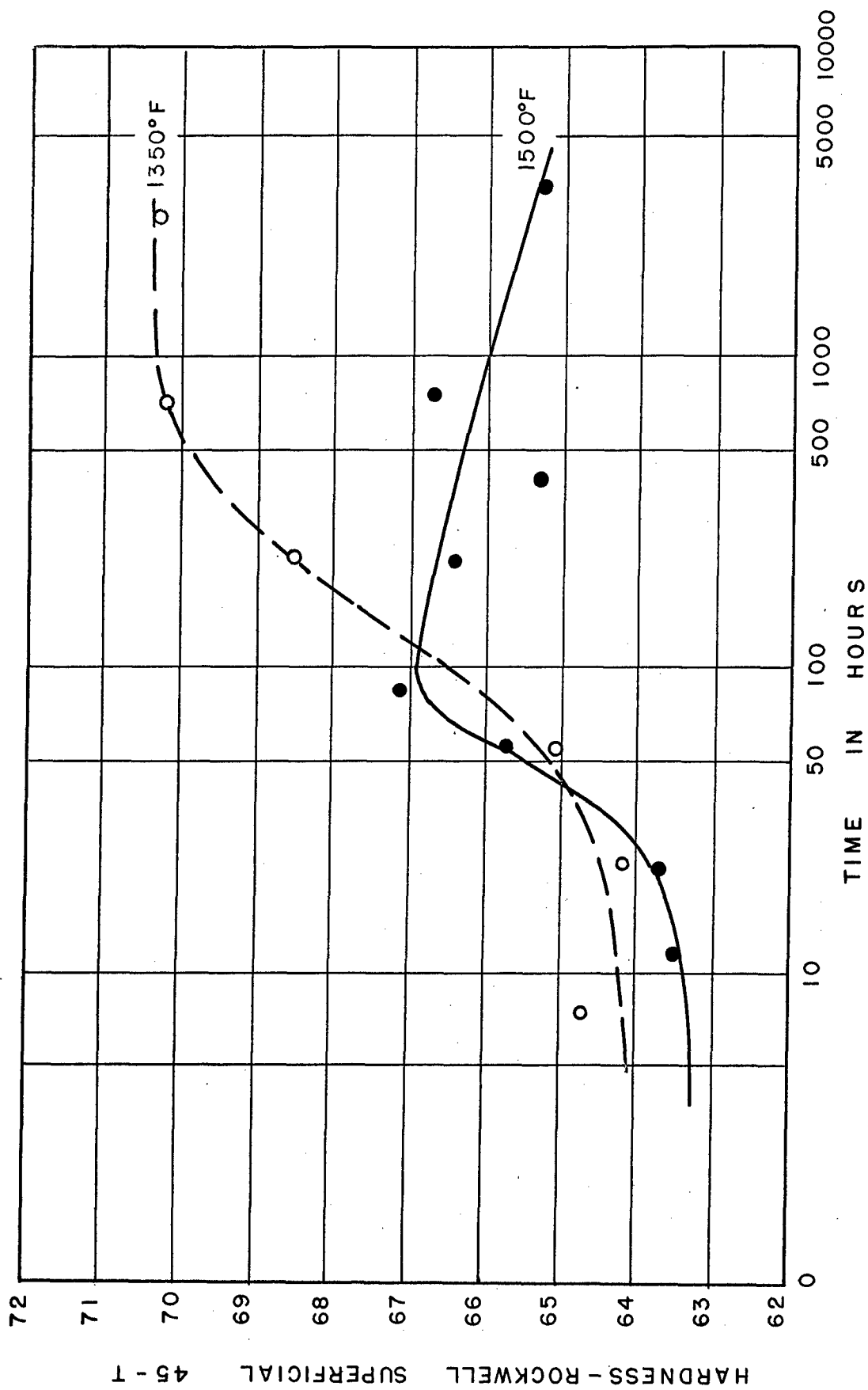


FIG. 8. — EFFECT OF TIME AND TEMPERATURE ON HARDNESS OF N-155.

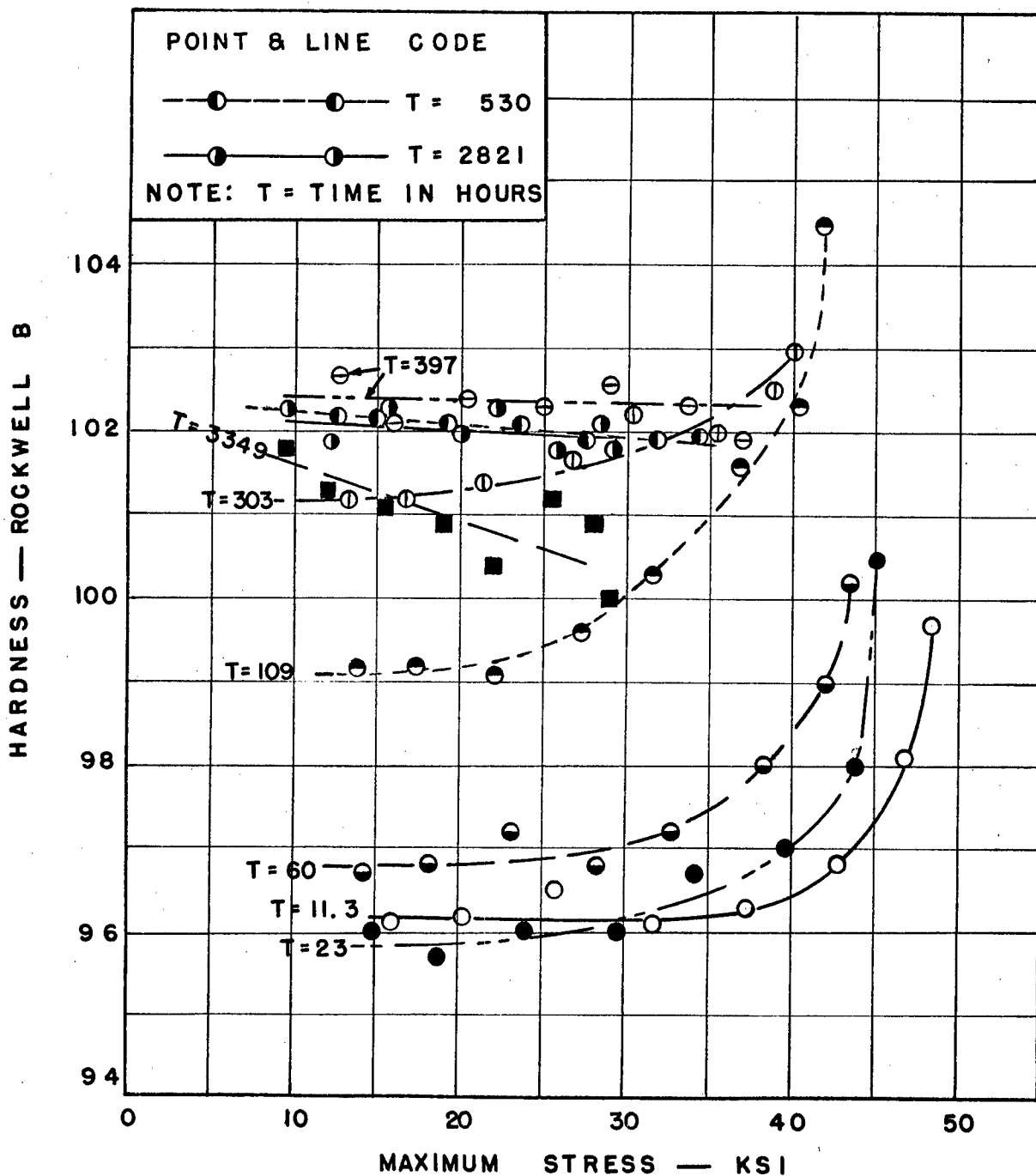


FIG. 9. HARDNESS VERSUS MAXIMUM STRESS FOR VARIOUS TIMES FOR N-155 AT 1350° F. STRESS RATIO 0.67; (CURVES CORRECTED FOR VARIANCE IN HARDNESS OF UNTESTED SPECIMENS).

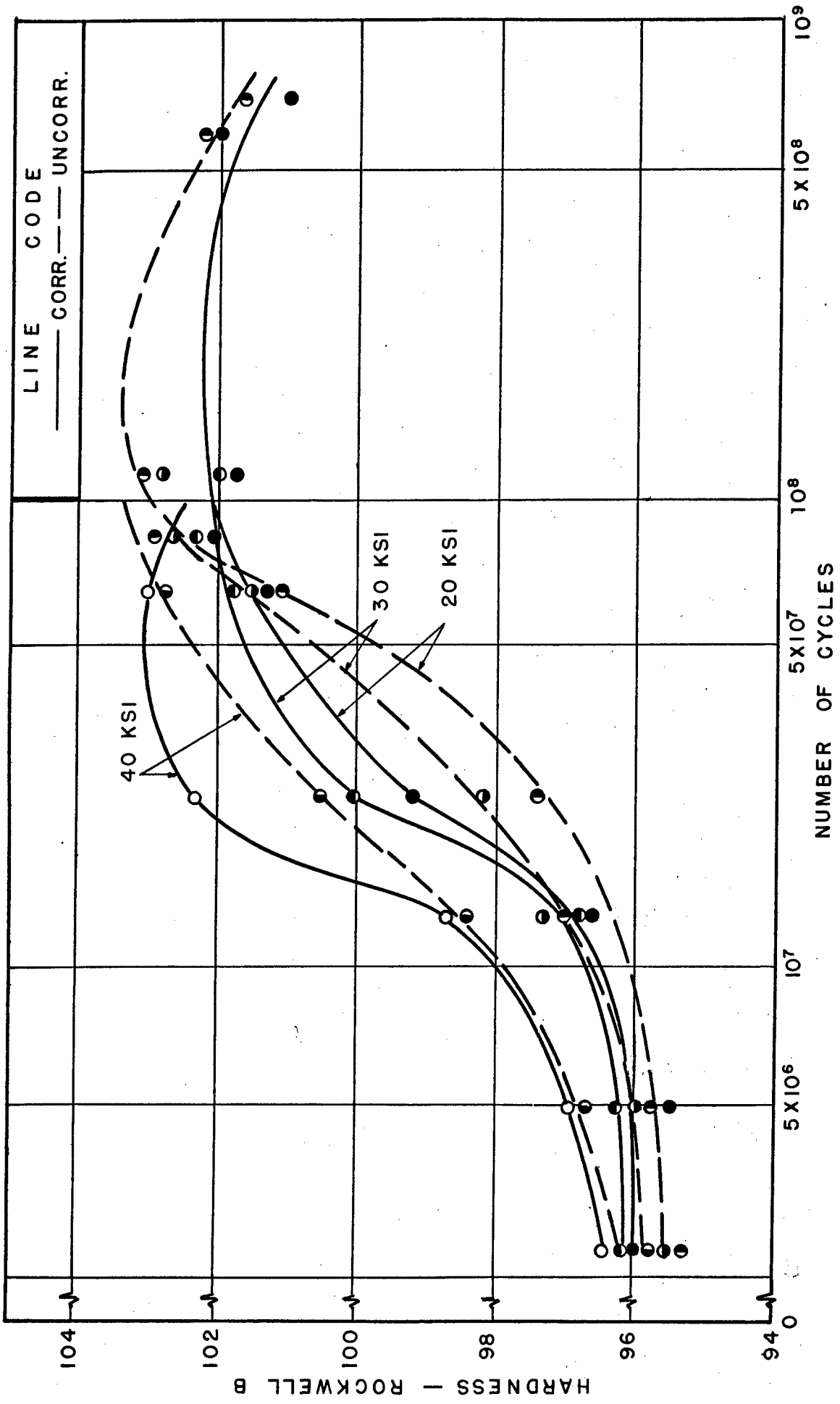


FIG. 10. EFFECT OF COMBINED MEAN AND REVERSED STRESS (STRESS RATIO 0.67) ON HARDNESS OF N-155 AXIAL STRESS SPECIMENS AT 1350°F (SHOWING CURVES CORRECTED AND UNCORRECTED FOR VARIANCE IN HARDNESS OF UNSTRESSED SPECIMENS.)

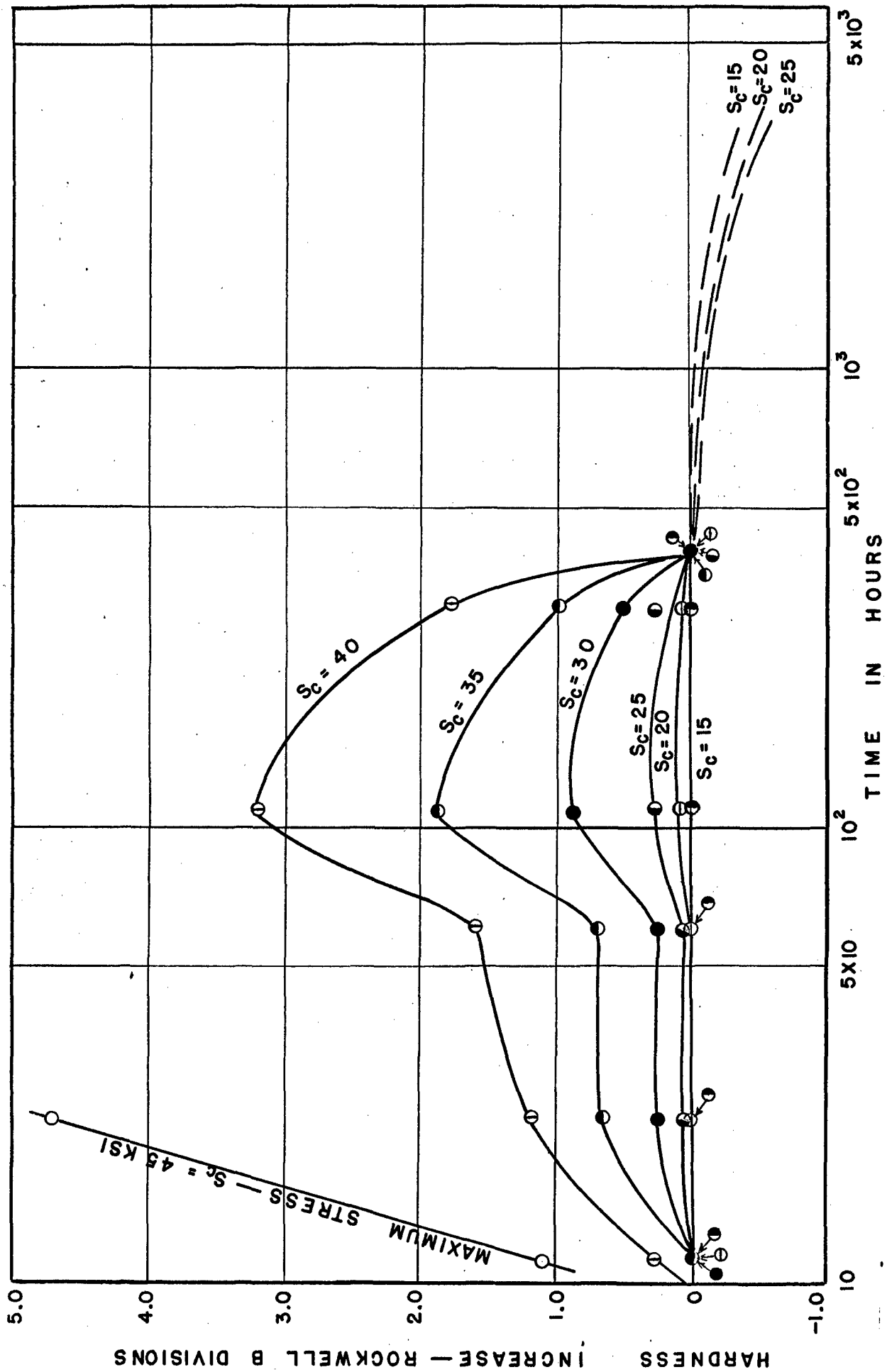


FIG. II.- INCREASE IN HARDNESS WITH TIME FOR DIFFERENT LEVELS OF MAXIMUM STRESS FOR N-155 AT 1350° F. AND STRESS RATIO 0.67

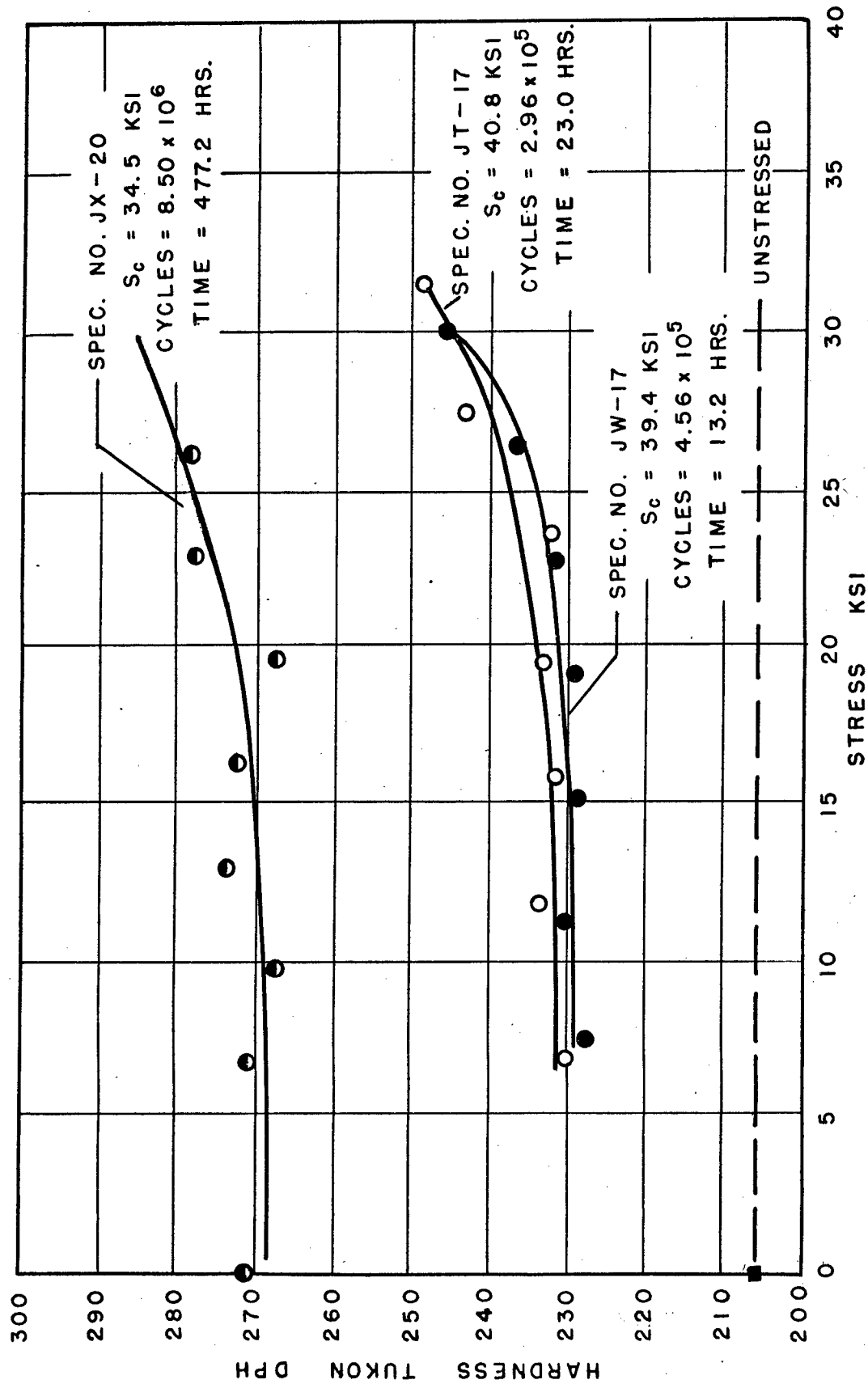


FIG.12. HARDNESS VS. STRESS FOR N-155 ROTATING BEAM SPECIMENS AT 1350°F.

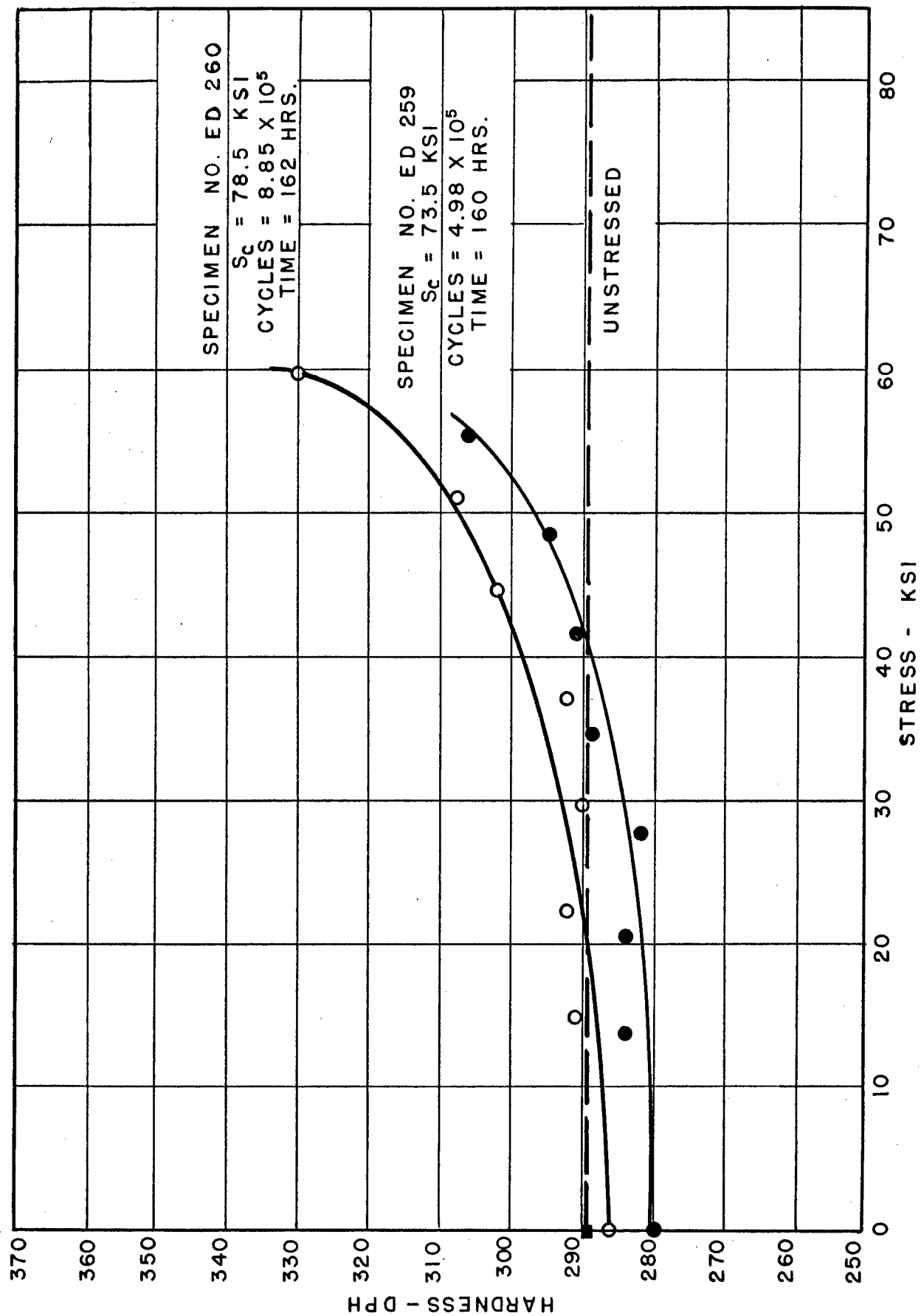


FIG.13. HARDNESS VS. STRESS FOR S-816 ROTATING BEAM SPECIMENS AT 900°F.

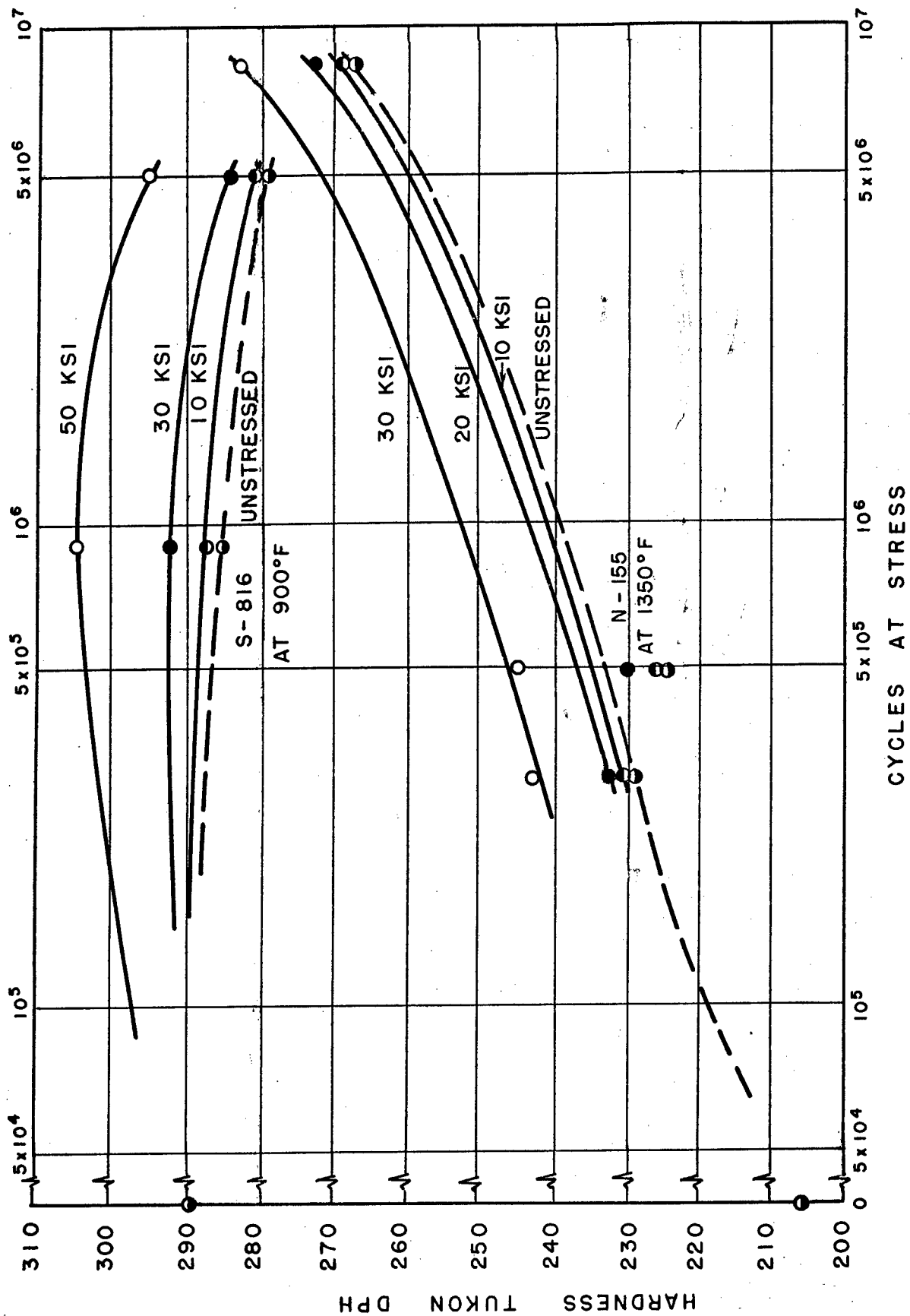


FIG.14. EFFECT OF REVERSED STRESS ON HARDNESS OF N-155 AND S-816 ROTATING BEAM SPECIMENS AT 1350°F AND 900°F, RESPECTIVELY.